Insertional Inactivation of the *menG* Gene, Encoding 2-Phytyl-1,4-Naphthoquinone Methyltransferase of *Synechocystis* sp. PCC 6803, Results in the Incorporation of 2-Phytyl-1,4-Naphthoquinone into the A_1 Site and Alteration of the Equilibrium Constant between A_1 and F_X in Photosystem I[†]

Yumiko Sakuragi,[‡] Boris Zybailov,[‡] Gaozhong Shen,[‡] A. Daniel Jones,[§] Parag R. Chitnis,[||] Art van der Est,[#] Robert Bittl,[$] Stephan Zech,[⊥] Dietmar Stehlik,[⊥] John H. Golbeck,[‡,*] and Donald A. Bryant[‡,*]

Department of Biochemistry and Molecular Biology, The Pennsylvania State University, University Park, Pennsylvania 16802, USA, Department of Chemistry, The Pennsylvania State University, University Park, Pennsylvania 16802, USA, Department of Biochemistry, Biophysics and Molecular Biology, Iowa State University, Ames, Iowa 50011, USA, Max Volmer Institut, Technische Universität Berlin, D-10623 Berlin, Germany, Fachbereich Physik, Freie Universität Berlin, D-14195 Berlin, Germany, and Department of Chemistry, Brock University, St. Catharines, Ontario, Canada, L2S 3A1

Received June 20, 2001; Revised Manuscript Received October 24, 2001

ABSTRACT: A gene encoding a methyltransferase (*menG*) was identified in *Synechocystis* sp. PCC 6803 as responsible for transferring the methyl group to 2-phytyl-1,4-naphthoquinone in the biosynthetic pathway of phylloquinone, the secondary electron acceptor in photosystem I (PS I). Mass spectrometric measurements showed that targeted inactivation of the *menG* gene prevented the methylation step in the synthesis of phylloquinone and led to the accumulation of 2-phytyl-1,4-naphthoquinone in PS I. Growth rates of the wild-type and the *menG* mutant strains under photoautotrophic and photomixotrophic conditions were virtually identical. The chlorophyll *a* content of the *menG* mutant strain was similar to that of wild type when the cells were grown at a light intensity of 50 μE m^{-2} s^{-1} but was slightly lower when grown at 300 μE m^{-2} s^{-1}. Chlorophyll fluorescence emission measurements at 77 K showed a larger increase in the ratio of PS II to PS I in the *menG* mutant strain relative to the wild type as the light intensity was elevated from 50 to 300 μE m^{-2} s^{-1}. CW EPR studies at 34 GHz and transient EPR studies at multiple frequencies showed that the quinone radical in the *menG* mutant has a similar overall line width as that for the wild type, but consistent with the presence of an aromatic proton at ring position 2, the pattern of hyperfine splittings showed two lines in the low-field region. The spin polarization pattern indicated that 2-phytyl-1,4-naphthoquinone is in the same orientation as phylloquinone, and out-of-phase, spin−echo modulation spectroscopy shows the same $P700^+$ to Q^- center-to-center distance as in wild-type PS I. Transient EPR studies indicated that the lifetime for forward electron transfer from Q^- to F_X is slowed from 290 ns in the wild type to 600 ns in the *menG* mutant. The redox potential of 2-phytyl-1,4-naphthoquinone is estimated to be 50 to 60 mV more oxidizing than phylloquinone in the A_1 site, which translates to a lowering of the equilibrium constant between Q^-/Q and F_X^-/F_X by a factor of ca. 10. The lifetime of the $P700^+$ $[F_A/F_B]^-$ backreaction decreased from 80 ms in the wild type to 20 ms in the *menG* mutant strain and is evidence for a thermally activated, uphill electron transfer through the quinone rather than a direct charge recombination between $[F_A/F_B]^-$ and $P700^+$.

Photosystem I (PS I)[1] in cyanobacteria is a membrane-integrated, pigment−protein complex consisting of 12 protein subunits (PsaA through PsaF, PsaI through PsaM, and PsaX) and a variety of cofactors including 96 molecules of chlorophyll *a* (Chl *a*), two molecules of 2-methyl-3-phytyl-1,4-naphthoquinone (phylloquinone), three [4Fe-4S] clusters, and 22 molecules of β-carotene (*1*). After the absorption of a photon by one of the antenna chlorophylls, charge separation takes place between a special pair of Chl *a* molecules (P700) and a Chl *a* monomer (A_0). The charge-

[†] This work was supported by grants from the National Science Foundation (MCB-9723661 and MCB-0117079 to J.H.G., MCB-9723001 to P.R.C., and MCB-9723469 to D.A.B.) and by the Deutsche Forschungsgemeinschaft (SFB 498, TP A3, and SPP "High Field EPR"), Fonds der Chemischen Industrie (to R.B.) and grants from the Natural Sciences and Engineering Research Council, The Canada Foundation for Innovation, and The Ontario Innovation Trust (to A.vdE.).

* To whom correspondence should be addressed. Tel: 814 865 1992; fax: 814 863 7024; e-mail: dab14@psu.edu.

[‡] Department of Biochemistry and Molecular Biology, The Pennsylvania State University.

[§] Department of Chemistry, The Pennsylvania State University.

[||] Iowa State University.

[$] Technische Universität Berlin.

[⊥] Fachbereich Physik, Freie Universität Berlin.

[#] Brock University.

[1] Abbreviations: PS, photosystem; CW, continuous wave; EPR, electron paramagnetic resonance; ENDOR, electron nuclear double resonance; HPLC, high performance liquid chromatography; MS, mass spectroscopy; PCR, polymerase chain reaction; SDS, sodium dodecyl sulfate; Tricine, *N*-[2-hydroxy-1,1-bis(hydroxymethylethyl]glycine; bp, base pair(s); kb, kilo-base; Chl, chlorophyll; phylloquinone, 2-methyl-3-phytyl-1,4-naphthoquinone or 2-methyl-3-(3,7,11,15-tetramethyl-2-hexadecenyl)-1,4-naphthalenedione; ORF, open reading frame.

10.1021/bi011297w CCC: $22.00
Published on Web 12/11/2001

separated state is stabilized on the donor side by electron transfer from plastocyanin or cytochrome c_6 to $P700^+$ and on the acceptor side by electron transfer to phylloquinone in the A_1 site, through the iron−sulfur clusters at F_X, F_A, and F_B, and ultimately to ferredoxin or flavodoxin. This light-driven enzyme is therefore a cytochrome c_6/plastocyanin: ferredoxin/flavodoxin oxidoreductase that provides reducing power to the cell in the form of NADPH.

Two molecules of phylloquinone are present per P700 in PS I complexes of *Synechocystis* sp. PCC 6803 and *Synechococcus* sp. PCC 7002 (*2*−*5*). Both quinones have been located on the 2.5 Å resolution electron density map of *Synechococcus elongatus* (*1*), and there is good agreement with EPR studies that provide distance (*6*) and orientation (*7*, *8*) information of the EPR-active quinone. For example, the same orientation of the carbonyl oxygen bonds of phylloquinone, tilted ca. 30 degrees from the membrane plane, is deduced from the orientation of the magnetic g_{xx} axis (ref *8* and earlier references therein) and the electron density map (*5*). Phylloquinone is structurally related to menaquinone-9 (2-methyl-3-nonaprenyl-1,4-naphthoquinone). Both have 2-methyl-1,4-naphthoquinone core structures with a poly-isoprenoid chain at the C_3 ring position: menaquinone has an unsaturated C_{45} isoprenoid chain, while phylloquinone has a partially saturated C_{20} chain. Because of their similarities in structure, it is likely that the phylloquinone biosynthetic pathway is similar to the menaquinone biosynthetic pathway in *Escherichia coli* (*9*). The biosynthetic pathway of phylloquinone is interesting for two reasons. First, the genes and enzymes of this pathway have not yet been completely characterized in cyanobacteria. Second, knowledge of this pathway should enable one to devise biological and chemical strategies to modify the quinone present in the A_1 site.

We recently proposed a pathway for phylloquinone biosynthesis in *Synechocystis* sp. PCC6803, which includes the genes *menA*, *menB*, *menD*, *menF*, and *menG* (*9*). Inactivation of the *menA* and *menB* genes, predicted to encode 1,4-dihydroxy-2-naphthoic acid phytyltransferase and 1,4-dihydroxy-2-naphthoate synthase, respectively, prevented the synthesis of phylloquinone and led to the incorporation of plastoquinone-9 into the A_1 site of PS I (*10*). Plastoquinone-9 is the secondary quinone acceptor of photosystem II (PS II) and additionally functions as the molecule that shuttles electrons to the cytochrome b_6/f complex. We reported that plastoquinone-9 is present in the A_1 site of the PS I with the same orientation and asymmetric spin density distribution as phylloquinone in wild-type PS I (*10*). Plastoquinone-9 is a benzoquinone with a C_{45} isoprenoid tail and is structurally and functionally only distantly related to phylloquinone. The observations that plastoquinone-9 could be inserted into the A_1 site and could function in lieu of phylloquinone indicate that this binding site is not specific for menaquinones. Rather, the properties of the quinone appear to be conferred largely by the protein environment of the A_1 site rather than by the identity of the quinone (*11*).

The object of this study is the protein encoded by ORF sll1653, which was originally identified as *gerC2*. This ORF is homologous to *menG*, which encodes a methyltransferase in *E. coli* and other bacteria. In *Synechocystis* sp. PCC 6803, this gene is anticipated to encode a 2-phytyl-1,4-naphthoquinone methyltransferase (*9*). 2-Phytyl-1,4-naphthoquinone differs from phylloquinone only by the absence of a methyl group at ring position C_2 and by a higher redox potential than phylloquinone (*12*). The relationship between the molecular structure of this quinone and the axes of the molecular *g*-tensor is depicted in Figure 1.

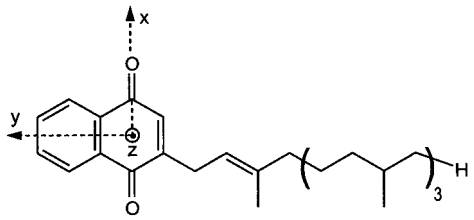

FIGURE 1: Relationship between the molecular structure of 2-phytyl-1,4-naphthoquinone and the axes of the electronic *g*-tensor. The axes of the electronic *g*-tensor of 2-phytyl-1,4-naphthoquinone (indicated by arrows) are parallel to the molecular axes system.

This study has two aims. The first is to confirm that sll1653 codes for the methyl transferase responsible for synthesizing 2-methyl-3-phytyl-1,4-naphthoquinone from 2-phytyl-1,4-naphthoquinone. Indeed, we found that inactivation of ORF sll1653 resulted in the synthesis of PS I complexes containing 2-phytyl-1,4-naphthoquinone in the A_1 site. The second is to study the roles of the methyl group in quinone binding and electron transfer in PS I. Here, we show that 2-phytyl-1,4-naphthoquinone is present in the A_1 site with the same orientation and asymmetric spin density distribution as phylloquinone in native PS I. We also report that 2-phytyl-1,4-naphthoquinone functions in forward electron transfer with some attendant alteration of the PS I activity and electron-transfer kinetics.

MATERIALS AND METHODS

Generation of the menG Mutant Strain of Synechocystis sp. PCC 6803. To generate the construct for inactivation of the *menG* gene, a 1.2-kb DNA fragment containing the sll1653 open reading frame was amplified through PCR from the genome of the *Synechocystis* sp. PCC 6803. For cloning convenience, a new *Eco*RI site was created at the 3′-end primer by changing one nucleotide. The PCR-amplified DNA fragment was cloned into plasmid pUC19 and confirmed by sequencing. To inactivate the *menG* gene, a 1.3-kb kanamycin-resistance cartridge encoded by the *aph*II gene was inserted into the *Kpn*I site in the *menG* gene. The resulting plasmid was linearized by digestion with *Eco*RI and was used to transform *Synechocystis* sp. PCC 6803 wild-type cells. The transformation and the screening of transformants were carried out as described in ref *13*. After several rounds of restreaking to single colonies, full segregation of the *menG::aphII* and *menG* alleles was verified by PCR and Southern blot-hybridization analyses.

Growth of the menG Mutant Strain of Synechocystis sp. PCC 6803. Wild-type *Synechocystis* sp. PCC 6803 was grown in medium B−HEPES (*13*), and the *menG* mutant cells were grown in B−HEPES supplemented with 50 μg mL^{-1} kanamycin. The growth temperature was maintained at 32 °C, and the light intensity was adjusted to 50, 150, and 300 $\mu E\ m^{-2}\ s^{-1}$ by adding fluorescent lamps or by shielding with filter paper as required. For photomixotrophic growth, medium B−HEPES was supplemented with 5 mM glucose. Growth of the cells was monitored by measuring the absorbance at 730 nm using a Cary-14 spectrophotometer

that had been modified for computerized data acquisition by On-Line Instruments, Inc. (Bogart, GA). Cells from a liquid starter culture in the exponential phase ($A_{730\ nm} < 0.7$) were adjusted to the same initial cell density ($A_{730\ nm} = 0.05$) for growth-rate measurements. The liquid cultures were bubbled with 1% (v/v) CO_2 as previously described (*13*).

DNA Isolation, PCR, and Southern Blotting. Chromosomal DNA from *Synechocystis* sp. PCC 6803 wild-type and mutant strains was isolated as previously described (*13*). PCR primers used to amplify the *menG* DNA fragment for evaluation of the *menG* alleles were positioned as shown in the Figure 2. The sizes of the PCR products from the wild-type and *menG* mutant strains were determined by agarose gel electrophoresis. For Southern blot-hybridization analysis, the chromosomal DNAs were subjected to restriction enzyme digestion, agarose gel electrophoresis, and capillary transfer to nitrocellulose membranes. Hybridization probes were generated by labeling the wild-type *menG* PCR fragment with the random-primed DNA labeling kit (Boehringer-Mannheim, Indianapolis, IN). Hybridization conditions and detection were performed as previously described (*14*).

Chlorophyll Extraction and Analysis. Chlorophyll was extracted from whole cells, thylakoid membranes, and PS I particles with 100% methanol, and the concentration was determined spectrophotometrically as described in ref *15*.

Isolation of Thylakoid Membranes and PS I Particles. Thylakoid membranes were isolated from cells in late exponential growth phase as described previously (*13*). Cells were broken at 4 °C by three passages through a French pressure cell at 124 MPa. The thylakoid membranes were resuspended and solubilized for 2 h at 4 °C in the presence of 1% (w/v) *n*-dodecyl-β-D-maltoside. PS I complexes were separated from other membrane components by centrifugation on 5−20% (w/v) sucrose gradients containing 0.05% *n*-dodecyl-β-D-maltoside in the buffer. Further purification was achieved by a second centrifugation on sucrose gradients in the absence of *n*-dodecyl-β-D-maltoside. Only trimeric PS I complexes were used in these studies (*16*).

SDS−Polyacrylamide Gel Electrophoresis Analysis. Methods used for SDS−polyacrylamide gel electrophoresis were identical to those previously described (*14*). A Tricine/Tris discontinuous buffer system was used to resolve the polypeptide composition of the PS I complexes prepared from the wild type and the *menG* mutant strains of *Synechocystis* sp. PCC 6803 (*17*). The separating gel contained 16% (w/v) acrylamide and 6 M urea, and the resolved proteins were visualized by silver staining (*18*).

Analysis of Quinones by High Performance Liquid Chromatography and Mass Spectrometry. For extraction of quinones, PS I complexes isolated from the wild-type and *menG* mutant strains were exchanged into distilled water by dialysis for 4 h and lyophilized. The pigments were extracted from the lyophilized samples with 1:1 (v/v) acetone:methanol at 4 °C, vacuum-dried at room temperature in the dark, and resuspended in 100% methanol. The extracts were separated by reverse-phase, high performance liquid chromatography (HPLC) using a C18 column as previously described (*9*). Eluents were analyzed after atmospheric-pressure chemical ionization with a Perseptive Biosystem Mariner time-of-flight mass spectrometer operated in the negative-ion mode.

Flavodoxin Photoreduction. Steady-state rates of flavodoxin reduction were measured in the PS I complexes isolated from the wild-type and *menG* mutant strains as previously described (*19*). Cyanobacterial flavodoxin was overexpressed in *E. coli* (*20*) and purified as described (*21*). PS I trimers were resuspended to a final concentration of 5 μg of Chl mL^{-1} in 50 mM Tris buffer, pH 8.0, containing 50 mM $MgCl_2$, 15 μM cytochrome c_6, 15 μM flavodoxin, 6.0 mM sodium ascorbate, and 0.05% *n*-dodecyl-β-D-maltoside. Measurements were made by monitoring the rate of change in the absorption at 467 nm using a modified Cary 219 spectrophotometer fitted with a 465 nm interference filter on the surface of the photomultiplier. The four-sided clear cuvette was illuminated from both sides using high intensity, red light-emitting diodes (LS1, Hansatech Ltd., Norfolk, UK). Initial rates of the reaction were recorded under various light intensities and plotted as a function of the light intensity to assess the relative efficiency of forward electron transfer to flavodoxin.

77 K Fluorescence Emission Spectra. Fluorescence emission spectra were measured at 77 K using a SLM 8000C spectrofluorometer as described in ref *14*. Cells in the exponential phase of growth were harvested and resuspended in 25 mM HEPES/NaOH, pH 7.0, containing 60% glycerol. Samples were adjusted to equal cell density ($OD_{730\ nm} = 1.0$) prior to freezing in liquid nitrogen. The excitation wavelength was 440 nm, the excitation slit width was 4 nm, and the emission slit width was 2 nm. Each spectrum shown is the average of four spectra.

Q-band CW EPR of Photoaccumulated PS I Complexes. Photoaccumulation experiments were performed using a Bruker ER300E spectrometer and an ER 5106-QT resonator equipped with an opening for in-cavity illumination similar to that described in ref *22*. Low temperatures were maintained with an ER4118CV liquid nitrogen cryostat and an ER4121 temperature controller. The microwave frequency was measured with a Hewlett-Packard 5352B frequency counter, and the magnetic field was measured with a Bruker ER035M NMR gaussmeter. The pH of sample was adjusted to 10.0 with 1.0 M glycine buffer, and sodium dithionite was added to a final concentration of 50 μM. After incubation for 10 min in the dark, the sample was placed into the resonator, and the temperature was adjusted to 205 K. The sample was illuminated for 40 min with a 20 mW He−Ne laser operating at 630 nm. A dark background spectrum was subtracted from the photoaccumulated spectrum. EPR spectral simulations were carried out on a 466 MHz Power Macintosh G3 computer using a Windows 3.1 emulator (SoftWindows 3.0, Insignia Solutions, UK) and SimFonia software (Bruker Analytik GMBH).

Time-Resolved EPR Spectroscopy at Multiple Frequencies. Transient EPR spectra as well as pulsed EPR/ENDOR data were obtained using the same instrumentation described earlier (*6*, *10*).

Flash-Induced Absorbance Changes at 811 nm. Transient absorbance changes were measured with a home-built, double-beam spectrophotometer described in (*23*). The samples were prepared at a chlorophyll concentration of 7 μM in 50 mM Tris buffer, pH 8.3. Measurements were made at pH 8.3 in 50 mM Tris buffer in the presence of 2 mM sodium ascorbate and 5 μM 2,6-dichlorophenolindophenol. The samples were measured in a quartz cuvette with a 1-cm path for the measuring light. The excitation beam was provided by a frequency-doubled Nd:YAG laser (532 nm)

with the flash energy attenuated to ca. 20 mJ using the Q-switch delay and neutral density filters. The measuring beam was provided by a 5 mW semiconductor laser operating at 811 nm. Kinetic analysis was performed using a nonlinear regression algorithm in Igor Pro (Wavemetrics, Lake Oswego, OR) as described earlier (*23*). All kinetic constants are reported as 1/*e* lifetimes (τ).

X-band Transient EPR Spectroscopy at Room Temperature. Transient EPR experiments at room temperature were carried out using a modified Bruker ESP 200 spectrometer equipped with a home-built, broad-band amplifier (bandwidth > 500 MHz) for direct detection experiments. Light excitation was provided by a Continuum YAG/OPO laser system operating at 680 nm and 1 Hz. The EPR signals were digitized using a LeCroy LT322 500 MHz digital oscilloscope and transferred to a PC for storage and analysis. The samples were measured using a flat cell and a Bruker rectangular resonator fitted with a piece of rough-surfaced glass in front of the window to provide optimal illumination. The response time of the system in direct detection mode is limited by the bandwidth of the resonator and is estimated to be ~50 ns; the decay of the spin polarization limits the accessible time range to times shorter than a few microseconds. The same setup was also used with field modulation and lock-in detection. In this mode, the response time is ~50 μs, but the sensitivity is much higher and the charge recombination can be monitored in the millisecond time range. In both modes of operation, full time/field data sets were collected and analyzed to determine the lifetimes of the species and their decay-associated spectra as described in detail in refs *11* and *24*.

RESULTS

Analysis of the Genotype of the menG Mutant Strain. As shown in Figure 2A, the *menG* gene (ORF sll1653) was inactivated by insertion of a 1.3-kb DNA cassette, encoding the *aphII* gene and conferring resistance to kanamycin, in the unique *KpnI* site within the coding sequence. Full segregation of the *menG* and *menG::aphII* alleles was confirmed by PCR amplification and by Southern blot-hybridization analyses of the genomic DNA. For PCR analysis, primers flanking the *menG* coding sequence (Figure 2A small arrows) were used to amplify the DNA fragments from the wild-type and the *menG::aphII* transformant genomic DNAs. As expected, a 1.2-kb fragment was amplified by the PCR reaction for the wild type (Figure 2B). For the *menG::aphII* mutant only a 2.5-kb fragment was amplified by PCR, and no DNA fragment with a size equal to that expected from the wild-type *menG* allele was detected. This result indicates that the mutant strain is homozygous for the *menG::aphII* gene interruption. To verify the *menG* mutation further, genomic DNA was isolated from the wild-type and the *menG* mutant strains and digested with restriction enzymes *BglII* and *HindIII* (see Figure 2A) for Southern blot-hybridization analysis. Hybridization was performed using the PCR product from the wild-type genome as the probe. As expected, a single hybridizing band of 1.6 kb was observed for the wild-type strain. For the *menG* mutant, two hybridizing bands of 1.1 and 1.8 kb were observed because of the *BglII* endonuclease cleavage of the Km^r cartridge. These results confirm that the mutant strain is homozygous and that the *menG::aphII* allele has fully segregated from the wild-type allele.

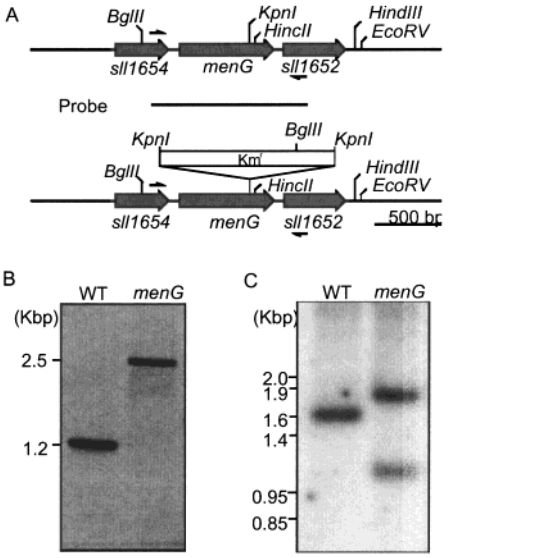

FIGURE 2: Construction and verification of the *menG* mutant strain of *Synechocystis* sp. PCC 6803. (A) Restriction map of the genomic region surrounding the *menG* gene in the wild type (top) and the *menG* mutant strain (bottom). The small arrows indicate the positions of the PCR primers used to amplify the *menG* coding region. (B) Electrophoretic analysis of the DNA fragments amplified from the genomic DNA of wild type and the *menG* mutant strain through PCR analysis. (C) Southern-blot hybridization analysis of the genomic DNA isolated from wild type and *menG* mutant strain. Chromosomal DNA was digested using restriction enzymes *Bgl*II and *Hin*dIII. As shown in top panel, a DNA fragment obtained by PCR from the wild-type genome was used as the hybridization probe.

High Performance Liquid Chromatography/Mass Spectrometry Analysis. To determine whether the *menG* gene is involved in phylloquinone biosynthesis, solvent-extracted quinone fractions from PS I complexes of the wild-type and *menG* mutant strains were subjected to orthogonal acceleration/time-of-flight mass spectrometry. Pigments and quinones extracted from the isolated PS I complexes were separated by reverse-phase HPLC, and the molecular mass of each eluted component was determined by mass spectrometry. In the wild-type complexes, phylloquinone was detected by its characteristic retention time, its absorption spectrum, and its mass/*z* of 450 (data not shown). In PS I complexes from the *menG* mutant strain, no compound absorbing at 270 nm eluted at this retention time, nor was a mass/z of 450 detected. Rather, a UV-absorbing component eluted near the retention time of chlorophyll *a* that had a mass/*z* of 436, which corresponds to the mass of 2-phytyl-1,4-naphthoquinone (data not shown).

Growth Rate under Photoautotrophic and Photomixotrophic Conditions. As indicated by HPLC and mass spectrometry, insertional inactivation of the *menG* gene resulted in the substitution of phylloquinone by 2-phytyl-1,4-naphthoquinone in PS I complexes. To measure the effectiveness of 2-phytyl-1,4-naphthoquinone in supporting photosynthesis, the growth rates of the wild-type and *menG* mutant strains were compared. The results are summarized in Table 1. Growth rates of the wild-type and the *menG* mutant strains were virtually the same under low (50 μE m^{-2} s^{-1}) and moderate (150 μE m^{-2} s^{-1}) light intensity, either in the presence or the absence of glucose (Table 1). When

Table 1: Doubling Time of *Synechocystis* sp. PCC 6803 Wild-Type and the *menG* Mutant Strains (hours)

strain	wild type	menG
photoautotrophic, 50 μE m^{-2} s^{-1} ($n = 4$)	9.8 ± 0.085	9.8 ± 0.95
photoautotrophic, 150 μE m^{-2} s^{-1} ($n = 3$)	8.1 ± 0.12	8.1 ± 0.25
photomixotrophic, 50 μE m^{-2} s^{-1} ($n = 4$)	7.9 ± 0.90	7.5 ± 0.47
photomixotrophic, 150 μE m^{-2} s^{-1} ($n = 4$)	5.6 ± 0.73	6.3 ± 0.56

cells were grown photoautotrophically, doubling times of both the wild-type and the *menG* mutant strains were ca. 10 h under low light intensity conditions and ca. 8 h under moderate light intensity conditions. When cells were grown photomixotrophically, the doubling times of the wild-type and the *menG* mutant strains were both ca. 8 h under low light intensity conditions, and ca. 6 h under moderate light intensity conditions. The observed differences in the growth rates between the wild-type and *menG* mutant strains were all within the range of error. These results suggest that under these illumination regimes, replacement of phylloquinone with 2-phytyl-1,4-naphthoquinone has no significant effect on growth.

PS II/PS I Ratio Measured by 77 K Fluorescence Emission Spectra. The ratios of PS II to PS I were compared by measuring 77 K fluorescence emission spectra of wild-type and *menG* mutant cells grown at various light intensities. The results are summarized in Figure 3. When cells were grown under low-light conditions, which is typical for *Synechocystis* sp. PCC 6803 (Figure 3A), the emission from PS I at 721 nm was much greater than that from PS II at 695 nm. When cells were grown at higher light intensities, an obvious decrease at 721 nm was found in the emission spectra of the *menG* mutant cells when compared to wild-type cells (Figure 3B and 3C). In wild-type cells the emission peak at 721 nm due to Chl *a* associated with PS I decreased approximately 10% in cells grown at a light intensity of 300 μE m^{-2} s^{-1} relative to cells grown at a light intensity of 50 μE m^{-2} s^{-1}, while emission peaks at 685 and 695 nm due to Chl *a* associated with PS II remained nearly constant. However, the peak amplitude at 721 nm decreased substantially in *menG* mutant cells grown at higher light intensities. The amplitude of this peak in cells grown at a light intensity of 300 μE m^{-2} s^{-1} was less than 70% that for cells grown at 50 μE m^{-2} s^{-1}. The PS II/PS I ratio is slightly higher in the *menG* mutant than in wild type when grown at 50 μE m^{-2} s^{-1} and significantly higher when grown at 300 μE m^{-2} s^{-1}. These results suggest that there may be either a defect in the assembly of PS I complexes or an accelerated degradation of PS I complexes in the *menG* mutant cells grown at high light intensities.

Chlorophyll Content of Whole Cells Grown at Various Light Intensities. The chlorophyll contents of wild-type and *menG* mutant cells grown under various light intensities were also determined (Table 2). When cells were grown under low or moderate light intensities (50 or 150 μE m^{-2} s^{-1}), the chlorophyll content of the *menG* mutant cells was similar to that of the wild-type cells. However, when the light intensity was increased to 300 μE m^{-2} s^{-1}, the chlorophyll content in the wild-type cells decreased to approximately 70% of the initial value (Table 2). A significantly lower value, approximately 58% of the value obtained at lower light intensities, was observed for *menG* mutant cells grown at a light intensity of 300 μE m^{-2} s^{-1}. This value is only

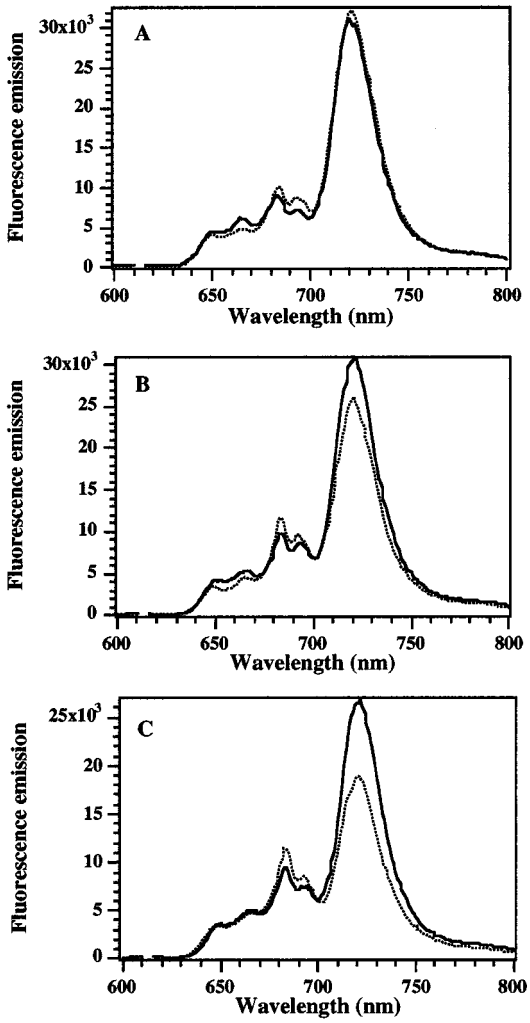

FIGURE 3: 77 K fluorescence emission spectra from whole cells of *Synechocystis* sp. PCC 6803. Chlorophyll fluorescence emission spectra were measured at 77 K for the whole cells of wild type (solid line) and the *menG* mutant strain (dotted line) grown under three different light intensities, (A) 50 μE m^{-2} s^{-1}, (B) 150 μE m^{-2} s^{-1}, (C) 300 μE m^{-2} s^{-1}. Each spectrum was recorded at the same cell density ($OD_{730\ nm} = 1.0$) and presented as the average of four measurements. The excitation wavelength was 440 nm.

Table 2: Chlorophyll Content in Cells Grown Photoautotrophically at 32 °C under Various Illumination Conditions[a]

light intensity (μE m^{-2} s^{-1})	μg of chlorophyll/$OD_{730\ nm}$ ($n = 3$)	
	wild type	menG
50	3.55 ± 0.24	3.40 ± 0.14
150	3.65 ± 0.21	3.40 ± 0.29
300	2.48 ± 0.34	1.98 ± 0.15

[a] Chlorophylls were extracted from whole cells with methanol. An extinction coefficient of 82 μg/mL^{-1} was used to calculate the chlorophyll content in 1 mL of the cultures with an optical density of 1.0 at 730 nm.

80% that of the wild-type strain under the same conditions, and this decrease can be correlated with the loss of fluorescence emission from PS I observable in the decreased emission at 721 nm in Figure 3. In combination, the results from Table 2 and Figure 3 suggest that the content of PS I complexes is lower in the *menG* mutant strain when cells were grown at high light intensity. This difference could be due to a defect either in biogenesis or in stability of the PS I complexes in the mutant strain.

Polypeptide Composition of Isolated PS I Trimers. To analyze whether the interruption of the *menG* gene has any effect on the PS I subunit composition, PS I complexes were analyzed by SDS−polyacrylamide gel electrophoresis, and polypeptides were visualized by silver staining. The 11 polypeptides detected in the wild type, PsaA though F and PsaI through M, were also found to be present in the *menG* mutant strain (data not shown). Likewise, no additional bands were observed in PS I complexes isolated from the *menG* mutant strain. These results indicate that the replacement of phylloquinone by 2-phytyl-1,4-naphthoquinone does not affect the polypeptide composition of the PS I complexes in the *menG* mutant strain.

EPR Spectroscopy of Q^- and $P700^+Q^-$. Figure 4 shows CW EPR spectra measured at 34 GHz (Q-band) of the photoaccumulated semiquinone radical (Q^-) in PS I complexes isolated from the wild-type (solid line, top) and the *menG* mutant strains (solid line, bottom). At this microwave frequency, the overall spectral line width of Q^- is similar to the wild type. Figure 5 shows transient, spin-polarized EPR spectra (X-, Q-, W-band) of the transient charge-separated $P700^+$ Q^- state in PS I complexes isolated from the wild-type (dashed line) and *menG* mutant strains (solid line). The two sets of spectra coincide quite well in the high-field region, which is dominated by the $P700^+$ contribution, but are noticeably different in the low-field region. The W-band spectrum indicates a slightly larger *g*-anisotropy for the PS I complexes of the *menG* mutant than for wild-type PS I complexes. This would be consistent with a slightly weaker H-bond and/or stronger $\pi-\pi$ stacking in the *menG* case, both of which would increase g_{xx} (see Figure 1 for the relationship between the molecular axes and the *g*-tensor axes). The best fit yields the principal values given in Table 3 which shows that only g_{xx} is altered in the in the *menG* mutant spectrum.

The expectation is that the CH_3 group will be replaced by an aromatic C−H fragment in the *menG* mutant. The pattern of hyperfine splitting should therefore be different from that of the wild-type. Indeed, the photoaccumulated CW spectrum (Figure 4) shows only two hyperfine lines in the low-field region rather than the usual four lines. Close inspection of the transient EPR spectrum (Figure 5) reveals that the main difference in the low-field region concerns the partially resolved hyperfine pattern. It is sufficiently resolved to permit a first qualitative analysis directly from the spectra. For the wild type, the characteristic hyperfine pattern due to the 1:3:3:1 quartet associated with a methyl group in ring position 2 is particularly obvious from both the photoaccumulated (Figure 4) and transient (Figure 5) Q-band spectra. The fact that it is partially resolved results from the increased spin density at the carbon ring position to which the methyl group is attached (specific to the semiquinone radical ion in the A_1 site). The center position of the doublet in the *menG* mutant is shifted downfield with respect to the center of the quartet in the wild type, i.e., toward the part of the spectrum associated with g_{xx}. Such a shift is expected with an altered orientation of the dominant hyperfine principal axis with respect to the molecular axis frame (see ref *8* for a complete description of the electronic and hyperfine axes of phylloquinone). Because the observed shift direction is toward the spectral features associated with g_{xx}, the dominant hyperfine axis will point more in the direction of the g_{xx} (Q) tensor axis in PS I complexes from the *menG* mutant, while it points more in the direction of the g_{yy} tensor axis in the PS I complexes of the wild type. Since the dominant hyperfine axis A_{11} of the CH_3 hyperfine tensor is usually almost parallel to the C−CH_3 bond axis, its direction is closer to (about 30 degrees off) the g_{yy} tensor axis. In contrast, the direction of the dominant hyperfine axis of the aromatic C−H fragment (which is expected to be in-plane and perpendicular to the C−H bond, see ref *26*, chapter 9) is closer to (about 30 degrees off) the g_{xx} (Q) tensor axis. The associated downfield shift of the center of the hyperfine doublet is therefore in agreement with the experimental result.

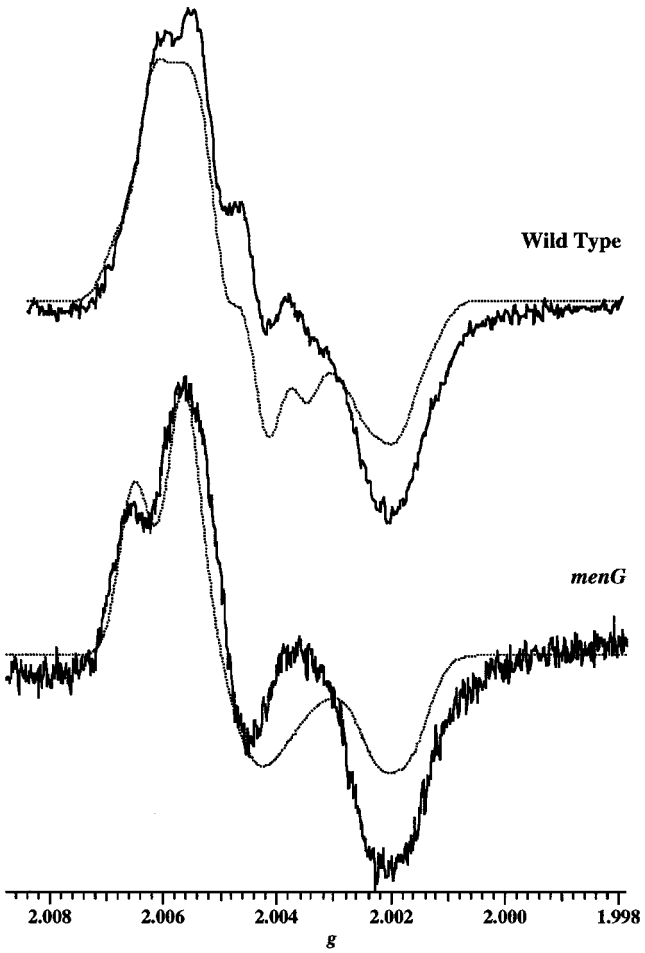

FIGURE 4: Photoaccumulated Q-band EPR spectra and simulations of PS I complexes from *Synechocystis* sp. PCC 6803. (A) wild type (solid line), and the simulated spectrum (dashed line). (B) *menG* mutant strain (solid line), and the simulated spectrum (dashed line). See text for details of the parameters of the simulation. The phyllosemiquinone anion radical is simulated using principal *g*-tensor values of $g_{zz} = 2.0022$, $g_{yy} = 2.0051$, and $g_{xx} = 2.0062$ and principal hyperfine A-tensor values of 9.0, 12.8, and 9.0 MHz for the three protons in the methyl group at the C_2 position (see ref *10*). The hyperfine splitting due to the remaining aromatic hydrogen atoms and methylene groups of the phytyl chain at the C_3 position remain unresolved and are included in the inhomogeneous line-broadening using line widths of 3.0, 6.0, and 4.0 G for each of the three g-tensor components. The 2-phytyl-1,4-naphthoquinone anion radical is simulated using the same principal *g*-tensor values and principal hyperfine tensor values of −15.5, −3.6, and −11.8 MHz for the single proton at the C_2 position. The deviations of the experimentally obtained spectra (solid line) from the simulated spectra (dashed line) seen in the mid- and high-field regions of both spectra are due to contamination by A_0^-.

Parameters for the Simulation of the EPR Spectrum of Q^-. To prepare for a quantitative simulation of the spectra,

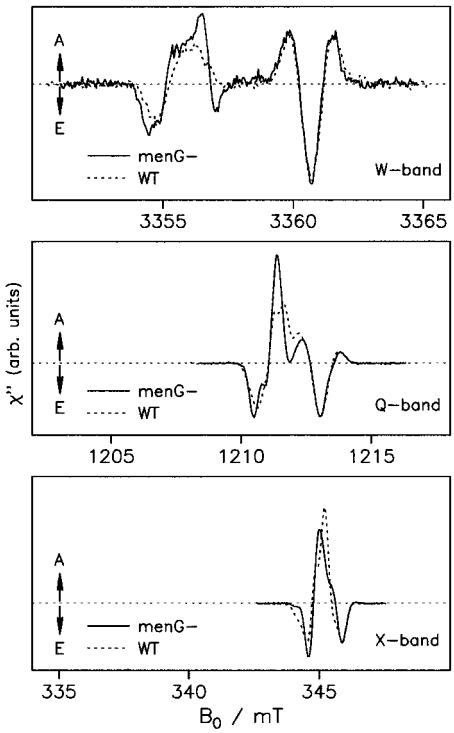

FIGURE 5: Transient spin-polarized EPR spectra (X-, Q-, and W-band) of the transient charge separated $P700^+ Q^-$ state in PS I trimers. Wild-type spectrum (dashed line) and *menG* mutant (solid line). The frequencies are from bottom to top: 9, 35, and 95 GHz. Experimental details same as described in ref *10*.

Table 3: Magnetic Parameters of Phylloquinone (A_1^-) and 2-Phytyl-1,4,-naphthoquinone (Q^-) in the A_1 Binding Site

	g-tensors[a]		
	g_{xx}	g_{yy}	g_{zz}
A_1^-[b]	2.00622	2.00507	2.00218
Q^-	2.00633	2.00507	2.00218
	HFC principal values (MHz)		
	A_{11}	A_{22}	A_{33}
$C-CH_3$ (A_1^-)[b]	12.8	9.0	9.0
C−H (Q^-)	-15.5 ± 0.5	-11.8 ± 0.5	<5

[a] The principal axes of the *g*-tensors are shown in Figure 1. [b] Ref *8* and references therein.

the following findings were taken into account. The spin polarization pattern shows that 2-phytyl-1,4-naphthoquinone has the same orientation in the A_1 site as native phylloquinone (Figure 5). The same P700 to A_1 center-to-center distance has been verified by out-of-phase spin−echo modulation spectroscopy (data not shown) (*6*, *10*). An independent determination of the hyperfine tensor components of the C−H fragment has been obtained from pulsed ENDOR spectroscopy of $P700^+ Q^-$ in the *menG* mutant (data not shown). The principal hyperfine tensor components are given in Table 3. While the two largest components, A_{11} and A_{22} are clearly resolved, the third component is buried in the manifold of lines in the center of the ENDOR spectrum and cannot be evaluated directly. However, simulations place an upper limit of 5 MHz on A_{33} as indicated in Table 3. This puts an upper limit of $A_{iso} \leq -10.8$ MHz on the isotropic hyperfine coupling constant and is consistent with the value of $A_{iso} = -10.3$ MHz for a $C-CH_3$ fragment,

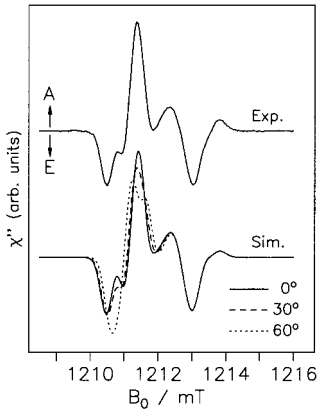

FIGURE 6: Simulations of the Q-band spectrum of the *menG* mutant carried out for various angles between the largest principal axis A_{11} and the g_{xx} axis. Top: experimental spectrum as in Figure 4 (middle). Bottom: simulations as described and with the parameters specified in the text (or otherwise unchanged from the parameter set used in ref *8*). The parameter variation concerns three different angles between the hyperfine axis associated with the largest principal value A_{11} and the g_{xx} axis.

which has similar McConnell Q-factors to a C−H fragment (see e.g., ref *26*, Table 6.1). If we ignore the Q-factor difference as indistinguishable within the experimental accuracy, the common value $A_{iso} = -10.3$ MHz gives for the third component: $A_{33} = -3.6$ MHz (see ref *8* for a table of parameters for simulations of the wild-type spectra).

Although the axis associated with the largest hyperfine component is expected to be in-plane and perpendicular to the C−H bond, this direction can be influenced by significant spin densities on neighboring molecular atoms such as the spin density which is known to reside on the carbonyl groups of the semiquinone radical. Therefore, simulations of the Q-band spectrum (Figure 6) were carried out for various angles between the largest principal axis A_{11} and the g_{xx} (Q) axis (in plane along the carbonyl bond direction). The A_{11} axis is perpendicular to the C−H bond direction when this angle is 30°. Indeed, of the simulations shown, the one for this value (Figure 6 bottom, long dashed curve) comes closest to the experimental spectrum (Figure 6, top). A slightly smaller angle than 30° improves the simulation somewhat indicating that there is only a weak influence on the orientation of the A-tensor axes from spin density on neighboring atoms. A satisfactory simulation of the photoaccumulated CW spectrum (Figures 4B, dotted line) is also obtained using the parameters derived from the spin-polarized spectra, i.e., by modifying the wild-type simulation (Figure 3A, dotted line), with the A-tensor of the methyl group replaced by that of an aromatic C−H fragment and using a larger g_{xx} value.

Kinetics of Forward Electron Transfer from A_1^- to F_X. Forward electron-transfer kinetics from the quinone to the iron sulfur clusters in PS I complexes isolated from the wild-type and the *menG* mutant strains are compared in Figures 7 and 8, which show spin-polarized EPR transients and decay-associated spectra, respectively. The transients in Figure 7 labeled a, b, and c were taken at the corresponding field positions indicated with labeled arrows in Figure 8. In wild-type PS I complexes, two consecutive spectra are observed as electron transfer from A_1^- to F_X occurs. At early times, an emission/absorption/emission (EAE) pattern due

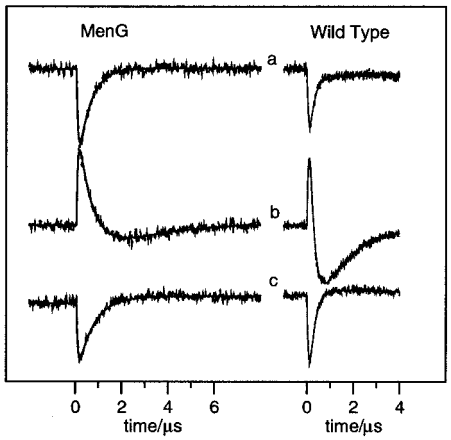

FIGURE 7: Spin-polarized EPR transients of the wild type and *menG* mutant. The traces a, b, and c were collected using direct detection at the field positions indicated by the similarly labeled arrows in Figure 8. The traces on the left of the figure are for *menG*, and those on the right are for the wild type. The electron transfer from Q^- to F_X is reflected in the decay of the signals at positions a and c and the transition from an absorptive (positive) to emissive (negative) signal at position b. All experiments were carried out at room temperature. Sample conditions as follows: isolated PS I trimers at 1.8 mg/mL Chl with 50 mM ascorbate and 25 μM DCPIP.

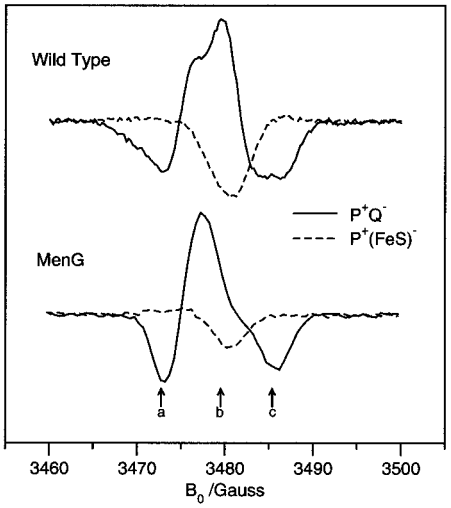

FIGURE 8: Decay-associated transient EPR spectra at ambient temperature. Spectra of the wild-type and *menG* mutant strains extracted from the full time/field datasets as described in detail in ref *24*. The solid curves correspond to the state $P700^+ Q^-$ while the dashed curves are the spectra of $P700^+ FeS^-$. The identity of the iron−sulfur center acceptor involved in the latter state is discussed in the text. The arrows labeled a, b and c indicate the field positions corresponding to the transients shown in Figure 7. Sample conditions and detection method are the same as for Figure 7.

to $P700^+ A_1^-$ is observed, which changes to an emissive spectrum due to $P700^+$ in the state $P700^+ FeS^-$ at later times. The identity of the iron−sulfur cluster partner to $P700^+$ in the state giving the late spectrum requires some discussion. It has been shown that the electron-transfer proceeds via F_X (*24*), which suggests the spectrum is due to $P700^+ F_X^-$. However, there is evidence (*27*) that electron transfer from F_X^- to F_A/F_B is faster than the transfer from A_1 to F_X. In this case, the late spectrum would be due to $P700^+ F_A^-$ and/or $P700^+ F_B^-$. Calculations (*28*) show the polarization patterns corresponding to $P700^+ F_X^-$, $P700^+ F_A^-$, and $P700^+ F_B^-$ show only minor differences. Thus, the state giving the late spectrum is labeled $P700^+ FeS^-$, and the identity of the iron−sulfur cluster is left open. In the kinetic traces (Figure 7), the electron transfer is seen most clearly at field position b (Figure 7, middle traces). The positive (absorptive) signal at early times is due to $P700^+ Q^-$, while the negative (emissive) signal at late times is due to $P700^+ FeS^-$. The electron transfer dominates the decay of the early signal, while relaxation of the spin polarization causes the decay of the late signal. At positions a and c, the intensity of the late signal is weak, and thus, the transients decay primarily with the electron transfer rate. As can be seen at all three field positions shown in Figure 7, the rate of electron transfer is considerably slower in the mutant than in the wild-type PS I complexes. For the mutant, a fit of the entire data set as described in ref *24* yields an average electron transfer (1/*e*) lifetime of 600 ± 100 ns. This is in comparison with a (1/*e*) lifetime of 290 ± 70 ns for the wild type.

Kinetics of Charge Recombination between $[F_A/F_B]^-$ and $P700^+$. The reduction of $P700^+$ was monitored at 811 nm after a brief laser flash in PS I complexes isolated from the wild-type and *menG* mutant strains. Because no soluble electron acceptors such as ferredoxin, flavodoxin, or methyl viologen were present, the reduction of $P700^+$ occurs by charge recombination with one or more bound electron acceptor(s). The kinetics of $P700^+$ reduction in PS I complexes from the wild-type strain (Figure 9A) were fitted by three exponentials with (1/*e*) lifetimes of 0.70, 30.7, and 94.7 ms. The latter two values are similar to the two lifetime components found previously for $P700-F_A/F_B$ complexes from *Synechocystis* sp. PCC 6803 and are attributed to charge recombination between $[F_A/F_B]^-$ and $P700^+$ (*23*). The first value is probably due to charge recombination between $P700^+$ and F_X^- in damaged PS I complexes that lack an intact PsaC subunit. The kinetics of $P700^+$ reduction in PS I complexes from the *menG* mutant strain (Figure 9B) were also fitted by two exponentials with (1/*e*) lifetimes of 10.3 and 29.3 ms. These values are attributed to charge recombination between $[F_A/F_B]^-$ and $P700^+$ and are ca. 3 times faster than the wild type. Even though the reason for the heterogeneity in $P700^+$ reduction is not understood, it is noteworthy that the two kinetic phases attributed to charge recombination between $[F_A/F_B]^-$ and $P700^+$ are equally slowed in the *menG* mutant samples.

The charge recombination kinetics between $[F_A/F_B]^-$ to $P700^+$ were also measured using slow time-resolution transient EPR with 100 kHz field-modulation. The decay-associated spectra for PS I trimers from the wild-type and *menG* mutant strains correspond to the amplitude of a biexponential function with the ratio of the two components kept constant over the whole field range (data not shown). For both the wild-type and *menG* complexes, the spectrum is the $P700^+$ contribution of $P700^+ [F_A/F_B]^-$ (the reduced iron−sulfur clusters cannot be observed at room temperature due to relaxation broadening). Thus, in the mutant complexes, electron transfer to the iron−sulfur centers occurs within the ~50 μs rise time of the lock-in detection. Although the spectra are identical, the associated decay curves differ considerably. The lifetime of the signal for the PS I complexes from the *menG* mutant is shorter than for the wild-type PS I complexes. A (1/*e*) lifetime of 100 ms is found for the major component of the $P700^+$ reduction of the wild-type sample, while a (1/*e*)

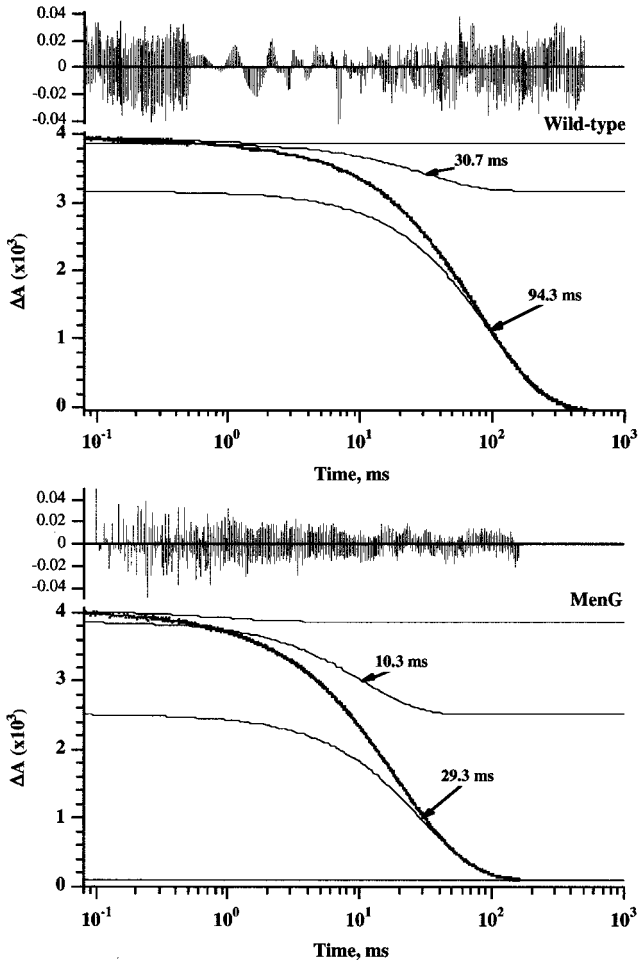

FIGURE 9: Flash-induced absorbance changes at 812 nm in PS I complexes isolated from *Synechocystis* sp. PCC 6803. The experimental data depicted shown as dots and the computer-generated exponential fits are shown as solid lines, with the lifetimes of the phase indicated. Top: $P700^+$ reduction kinetics in wild-type PS I complex. Bottom: $P700^+$ reduction kinetics in the *menG* PS I complex.

lifetime of 17 ms is found for the *menG* mutant (data not shown). These values roughly agree with the transient optical absorption measurements at 811 nm (see above) and probably differ only as a result of the lower sensitivity and thus poorer signal-to-noise ratio in the EPR transients. Since the EPR spectrum associated with the 17 ms component in PS I complexes of the *menG* mutant and the 100 ms component in the wild-type complexes are identical (data not shown), both lifetimes are due to the back reaction from $[F_A/F_B]^-$.

Steady-State Rates of Flavodoxin Reduction. Steady-state rates of flavodoxin reduction as a function of light intensity were measured for PS I complexes isolated from the wild-type and *menG* mutant strains to assess the relative efficiencies of forward electron transfer. The rates at saturating light intensity were determined by treating light as a substrate in a Michaelis−Menten kinetic analysis (Figure 10). The maximal rate of flavodoxin reduction was found to be 1527 ± 247 μmol mg Chl^{-1} h^{-1} for the wild-type PS I complexes and 1845 ± 399 μmol (mg of Chl)$^{-1}$ h^{-1} for the *menG* mutant PS I complexes. Assuming that 100 Chl molecules are present per P700 in all PS I complexes, these maximal rates of electron transfer correspond to 37.9 ± 6.2 e^- PS I^{-1} s^{-1} in the wild-type PS I complexes and 45.8 ± 8.4 e^- PS I^{-1} s^{-1} in the *menG* mutant PS I complexes. Although the value obtained for the PS I complexes of the *menG* mutant strain was slightly higher than that for the wild type, this difference is within the margin of error and therefore is not statistically significant (Figure 10). Hence, the steady-state rate of electron transport for the PS I complexes of the *menG* mutant, which contain 2-phytyl-1,4-naphthoquinone, was virtually identical to the steady-state rate of electron transfer for the phylloquinone-containing PS I complexes of the wild type.

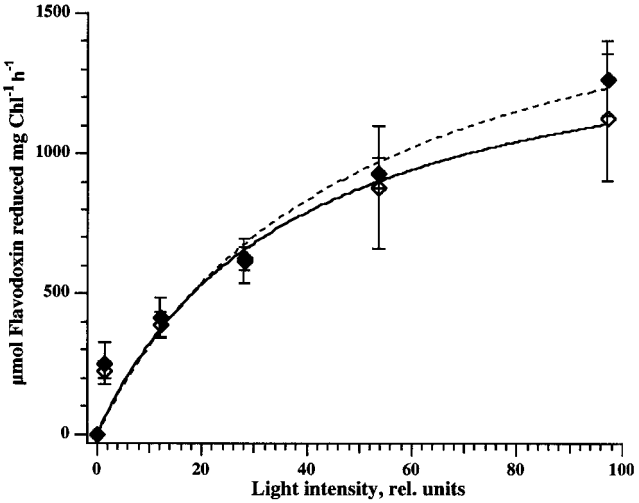

FIGURE 10: Steady-state rates of flavodoxin reduction in PS I complexes isolated from the wild-type and *menG* mutant strains. Seven independent measurements were performed for PS I complexes from each strain at each light intensity. The open and filled diamonds indicate the average values obtained for the complexes from the wild-type and *menG* mutant strains, respectively. The solid and dashed lines indicate fitted curves derived from the Michaelis−Menten equation for the rates obtained for PS I complexes from the wild-type and *menG* mutant strains, respectively. Bars on the data points indicate the standard deviations.

DISCUSSION

The *menG* gene, encoding the 2-phytyl-1,4-naphthoquinone (demethyphylloquinone) methyltransferase, was identified by targeted inactivation of ORF sll1653 in *Synechocystis* sp. PCC 6803. This open reading frame was originally annotated as *gerC2*, which encodes the spore germination protein C2 in *Bacillus subtilis* and other spore-forming bacteria (*29*, *30*). In fact, the deduced amino acid sequence for ORF sll1653 shows only 27% sequence identity to the *menG* gene product of *E. coli*. Targeted inactivation of ORF sll1653 was accomplished by insertion of kanamycin resistance cartridge in the coding region, which was confirmed by PCR amplification of the region containing the ORF and by Southern blot hybridization analysis. The presence of 2-phytyl-1,4-naphthoquinone in PS I complexes was confirmed by high performance liquid chromatography/mass spectrometry, and its function in electron transfer was demonstrated by CW and transient EPR spectroscopy. It can safely be concluded that ORF sll1653 in *Synechocystis* sp. PCC 6803 is *menG* and that this gene encodes 2-phytyl-1,4-naphthoquinone methyl transferase, the enzyme required for the last step of the phylloquinone biosynthetic pathway.

Despite the absence of phylloquinone and the presence of 2-phytyl-1,4-naphthoquinone in PS I, the growth rates of the

wild-type and the *menG* mutant cells were identical. As observed for many other cyanobacteria (*31*), the ratio of PS II to PS I is known to change in *Synechocystis* sp. PCC 6803 as a function of the light intensity during cell growth. An interesting observation was that the change in the ratio of PS II to PS I was more pronounced in the *menG* mutant strain than in the wild type as the light intensity was increased from 50 to 300 μE m^{-2} s^{-1}. In wild-type cells, the PS II to PS I ratio increased by a factor of 1.1, while in the *menG* mutant cells the PS II to PS I ratio increased by at least a factor of 2 as estimated from fluorescence emission spectra at 77 K. It is noteworthy that the overall chlorophyll content in the wild-type and *menG* mutant cells were similar at light intensities of 50 and 150 μE m^{-2} s^{-1}, and differed only at 300 μE m^{-2} s^{-1}. Therefore, the difference in the PS II to PS I ratio between wild type and the *menG* mutant strain can primarily be attributed to a change in the content of PS I, i.e., the number of PS I complexes declines in the *menG* mutant cells to a greater extent than in the wild-type cells as the light intensity is raised. By way of comparison, the *menA* and *menB* mutant strains, which contain plastoquinone-9 in the A_1 site of PS I, have been observed to grow significantly more slowly under photoautotrophic conditions and can only be grown under very low light intensity conditions ($<$20 μE m^{-2} s^{-1}). The ratio of PS II to PS I is already greater than 2:1 at low light intensity and might be expected to be even greater as the light intensity is increased (the cells, however, do not survive). Thus, it appears that *Synechocystis* sp. PCC 6803 must not exceed a 2:1 ratio of PS II to PS I before even moderate light intensities become lethal to the cells.

The time-resolved EPR results have demonstrated that 2-phytyl-1,4-naphthoquinone in the *menG* mutant enters the correct site and with the same orientation of the naphthoquinone headgroup as native phylloquinone in the wild type. The same orientation is deduced with the usual $\pm$10 degree accuracy from the same overall spin polarization pattern. In addition, this conclusion is confirmed in an independent manner, using the relative orientation of the respective partially resolved hyperfine tensors. The hyperfine principal axes for either an aromatic C$-$H fragment or a C$-$$CH_3$ fragment at the same ring position differ in a specific way in their orientation with respect to the molecular axes of the quinone. The respective axes orientations as determined in this work are consistent with the same orientation of the naphthoquinone headgroup in the A_1 site of both the *menG* mutant and wild type. More importantly, the same increased spin density (with respect to isotropic solution) is found for either the C$-$H or C$-$$CH_3$ fragment in both samples. For native phylloquinone, this fact is well established by ENDOR spectroscopy (*25*) and has been rationalized theoretically by density functional calculations (*32*). The same increased spin density observed here for the different C$-$H fragment at the same ring position adds a useful independent experimental verification. The larger spin density is due to an alternating spin density pattern along the ring positions, which in turn is the consequence of asymmetric H-bonding to mainly one of the two quinone carbonyl oxygens. The same alternating spin density pattern could be confirmed for even more ring positions in the case of plastoquinone-9 recruited to the A_1 site of the *menB* and *menA* mutants (*10*). Since the H-bonding pattern represents a key element of the protein$-$quinone interaction, it is significant that our results for the *menG* mutant confirm once more the characteristic spin density pattern for a modified quinone in the A_1 site. The different H-bonding pattern may also be a significant (although not the only) contributor to the large difference in redox potential known to exist for the same quinone acceptor (e.g., plastoquinone-9) acting in either type I (*menB* and *menA*) or type II (PS II) reaction centers.

To understand further the behavior of 2-phytyl-1,4-naphthoquinone in electron transfer, one must consider the redox potential of this quinone in the A_1 site. In aqueous solution, the $E(Q/Q^-)_7$ of 2-methyl-1,4-naphthoquinone is $-$203 mV vs NHE ,and the $E(Q/Q^-)_7$ of 2,3-dimethyl-1,4-naphthoquinone is $-$240 mV vs NHE (*33*). The $E(Q/Q^-)_7$ of 2-methyl-3-phytyl-1,4-naphthoquinone in aqueous solution (containing 5 M 2-propanol and 2 M acetone) is reported to be $-$170 mV (*33*). The presence of the second alkyl group *ortho* to the first therefore lowers the redox potential of the quinone by ca. 37 mV. However, the A_1 site is highly hydrophobic (*34*, *35*), and reduction potentials of quinones in organic solvent are probably more relevant to their properties in PS I. In dimethylformamide (DMF), the $E_{1/2}$ value for 2-methyl-1,4-naphthoquinone has been reported as $-$650 mV vs SCE and the $E_{1/2}$ value for 2,3-dimethyl-1,4-naphthoquinone has been reported as $-$746 mV vs SCE (*36*). The lower redox potential for the dimethyl quinone is logical chemically; a methyl group is an electron donor and should therefore destabilize the semiquinone radical in either aqueous solution or in organic solvent. A prenyl substituent on the quinone ring is not as effective as an electron donor as a second alkyl group and lowers the $E_{1/2}$ value by only 50 to 60 mV (*36*). For example, the $E_{1/2}$ of menaquinone-2 (2-methyl-3-all-*trans*-polyprenyl-1,4-naphthoquinone) is $-$709 mV vs SCE (to our best knowledge, the reduction potential of 2-phytyl-1,4-naphthoquinone in DMF is not available). Using the redox potentials for 2-methyl-1,4-naphthoquinone and 2,3-dimethyl-1,4-naphthoquinone as analogues for 2-phytyl-1,4-naphthoquinone and phylloquinone (both differ by the addition of one methyl group), the addition of a second methyl group *ortho* to the first should lower the redox potential by ca. 96 mV. If one further employs the concept of an "acceptor number", that was utilized in the interpretation of the properties for plastoquinone-9 in the *menA* and *menB* mutants (*11*), the redox potential of 2-phytyl-1,4-naphthoquinone in the A_1 site is estimated to be 61 mV more oxidizing than phylloquinone. An acceptor number corrects the $E_{1/2}$ value for the degree of nucleophilic (donor) or electrophilic (acceptor) properties of the solvent (*37*) and was employed earlier by Itoh (*35*) to estimate the redox potential of phylloquinone in the A_1 site of PS I. It is a dimensionless number that expresses the electrophilic properties of a solvent relative to $SbCl_5$.

The estimated redox potential of 2-phytyl-1,4-naphthoquinone in the A_1 site can now be compared to estimates based upon the experimentally measured rate of electron transfer. Forward electron transfer is ca. 3-times slower when 2-phytyl-1,4-naphthoquinone rather than phylloquinone occupies the A_1 site. According to the Moser-Dutton formulation (*38*), the rate of electron transfer in proteins depends on the Gibbs free energy between the donor$-$acceptor pair, the edge-to-edge distance between the donor$-$acceptor pair, and the reorganization energy. The distance between the

2-phytyl-1,4-naphthoquinone anion radical and $P700^+$ was experimentally determined here to be the same as the center-to-center distance between the phylloquinone anion radical and $P700^+$. The orientation of 2-phytyl-1,4-naphthoquinone relative to the membrane plane was also shown to be identical to that of phylloquinone. Hence, the edge-to-edge distance between 2-phytyl-1,4-naphthoquinone and F_X is likely the same as the distance between phylloquinone and F_X. It seems reasonable to assume similar reorganization energies when 2-phytyl-1,4-naphthoquinone and phylloquinone occupy the A_1 site, given that the only difference between the two quinones is the presence or absence of a single methyl group. Using the values of 11.3 Å for the edge-to-edge distance between the quinone and F_X (*39*), and a value of 0.7 eV for the reorganization energy, a (1/*e*) lifetime of ca. 290 ns for Q^- in the wild-type translates to an 81 mV difference in Gibbs free energy between Q^-/Q and F_X^-/F_X. Retaining the same values for the distance and reorganization energy, a (1/*e*) lifetime of 600 ns for Q^- in the *menG* mutant translates to a 28 mV difference in Gibbs free energy between Q^-/Q and F_X^-/F_X. According to this analysis, the addition of a methyl group to 2-phytyl-1,4-naphthoquinone lowers the redox potential of the quinone in the A_1 site by 53 mV. This value is only a rough estimate, especially given the uncertainties in the edge-to-edge distances between the cofactors and given the assumed (unchanged) reorganization energy of the site. Nevertheless, this value agrees quite well with the difference in redox potentials of 2-methyl-1,4-naphthoquinone and 2,3-dimethyl-1,4-naphthoquinone in organic solvents, especially after the correction for the site's "acceptor number". The replacement of phylloquinone by 2-phytyl-1,4-naphthoquinone would therefore lower the equilibrium constant between Q^-/Q and F_X^-/F_X from 27 to 3, a factor of ca. 10. Estimating the absolute redox potential of 2-phytyl-1,4-naphthoquinone in the A_1 site is somewhat more difficult because the redox potential of A_1 is not known with certainty. Three values have been published for the redox potentials of the Q^-/Q couple [−810 mV vs NHE (*40*), −800 mV vs NHE (*41*), and −754 mV vs NHE (*35*)]. If one uses the lower redox potentials, the replacement of phylloquinone by 2-phytyl-1,4-naphthoquinone would therefore raise the redox potential of the Q^-/Q couple to ca. −750 mV, a value that is probably still lower than the redox potential of the F_X^-/F_X couple (however, see ref *42* for an alternate view of a possible redox equilibrium between A_1 and F_X).

The kinetics of the reduction of $P700^+$ after a single flash represents dissipative charge recombination between $P700^+$ and the terminal electron acceptors $[F_A/F_B]^-$ in the absence of an acceptor such as ferredoxin or flavodoxin. It is not yet clear whether electron transfer is direct from $[F_A/F_B]^-$ to $P700^+$ or whether the electron travels backward by a thermally activated, uphill electron transfer through the quinone (*41*). The latter presupposes that each redox pair ($Q^-/Q \leftrightarrow F_X^-/F_X$; $F_X^-/F_X \leftrightarrow F_B^-/F_B$; $F_B^-/F_B \leftrightarrow F_A^-/F_A$) is described by an equilibrium constant that can be determined from the midpoint potentials of the acceptors. The large distance between P700 and the terminal iron−sulfur clusters [46 Å center-to-center distance from P700 to F_A; (*43*)] argues against the direct recombination mechanism, although experimental data to support thermally activated uphill electron transfer have been lacking. If the charge recombination between $[F_A/F_B]^-$ and $P700^+$ were direct, any change in the equilibrium constant between Q^-/Q and F_X^-/F_X should not affect the rate. However, if charge recombination between $[F_A/F_B]^-$ and $P700^+$ were to occur through backward electron transfer, then a change in the equilibrium constant between Q^-/Q and F_X^-/F_X should logically affect the rate. The equilibrium constant between Q^-/Q and F_X^-/F_X would be correspondingly higher as the redox potential of Q^-/Q were driven more negative, thereby resulting in a depopulation of reduced quinone. Consequently, the backreaction kinetics would be slower in the mutant than in the wild type. Conversely, the equilibrium constant between Q^-/Q and F_X^-/F_X would be correspondingly lower as the redox potential of Q^-/Q were driven more positive, thereby resulting in a repopulation of reduced quinone. Consequently, the backreaction kinetics in the mutant would be faster than in wild-type PS I complexes.

The latter description is precisely the behavior observed. The forward electron-transfer kinetics from Q^- to F_X becomes correspondingly slower as phylloquinone [1/*e* lifetime of 200 ns (*24*)], 2-phytyl-1,4-naphthoquinone (1/*e* lifetime of 600 ns) and plastoquinone-9 [1/*e* lifetime of 15 μs (*11*)] occupy the A_1 site. Conversely, the charge recombination kinetics between $[F_A/F_B]^-$ and $P700^+$ become more rapid as phylloquinone [1/*e* lifetime of 80 ms (*23*)], 2-phytyl-1,4-naphthoquinone (1/*e* lifetime of 20 ms) and plastoquinone-9 [1/*e* lifetime of 3 ms (*11*)] occupy the A_1 site. The trend among the wild type, *menA/menB*, and *menG* mutants therefore strongly supports the backward, through-carrier route of electron transfer for charge recombination. Since the redox potential of the quinone in the A_1 site influences the rate of charge recombination from the terminal electron acceptors to $P700^+$ as well as the forward electron transfer between the quinone and the terminal iron−sulfur clusters, this suggests that charge recombination occurs by thermally activated uphill electron transport through the secondary quinone acceptor in PS I. However, since it is possible that competing channels on the time scale of hundreds of milliseconds could exist for the charge recombination process between $[F_A/F_B]^-$ and $P700^+$, this conclusion should be considered tentative.

Finally, although the kinetics of electron transfer within PS I are altered when phylloquinone is replaced by 2-phytyl-1,4-naphthoquinone, these changes do not affect the growth rate of the organism. An explanation for this apparent discrepancy is that the slower rate of forward electron transfer from A_1^- to F_X is still not the rate-limiting step in the overall electron transfer reaction to flavodoxin (or probably to ferredoxin). Indeed, the maximal rate of flavodoxin reduction for the PS I complexes isolated from the *menG* mutant was virtually identical to that observed for wild-type PS I complexes. Analysis of the rate of electron donation from PS I to flavodoxin is complicated by the two-electron reduction using this acceptor. Since the potentials at pH 7 for the oxidized flavodoxin/flavodoxin semiquinone couple and the flavodoxin semiquinone/hydroquinone couple are −212 and −436 mV (*43*), respectively, it is likely that only the latter couple is physiologically relevant. Studies show that the reduction of flavodoxin semiquinone is biphasic; the fast first-order phase is electron transfer within a preformed complex, but the slower phase is concentration-dependent, with a second-order rate constant of 1.7×10^8 M^{-1} s^{-1}.

Given the nearly wild-type electron-transfer rates from cyt c_6 to flavodoxin in the *menG* mutant, it is clear that forward electron transfer continues to out-compete the faster back-reaction rate in the mutant. In this respect, one can consider that the PS I complex may represent an example of naturally selected "over-engineering", since the tolerances to changes in replacement of components with "suboptimal" ones still allows for a remarkable level of functionality of the bound electron-transfer cofactors.

ACKNOWLEDGMENT

The authors thank Prof. Dr. Wolfgang Lubitz for his generosity in allowing us to use his EPR facility.

REFERENCES

1. Jordan, P., Fromme, P., Witt, H. T., Klukas, O., Saenger, W. and Krauss, N. (2001) *Nature* 411, 909−917.
2. Biggins, J., and Mathis, P. (1988) *Biochemistry 27*, 1494−1500.
3. Malkin, R. (1986) *FEBS Lett. 208*, 343−346.
4. Schoeder, H. U., and Lockau, W. (1986) *FEBS Lett. 199*, 23−27.
5. Takahashi, Y., Hirota, K., and Katoh, S. (1985) *Photosyn. Res. 6*, 183−192.
6. Bittl, R., Zech, S. G., Fromme, P., Witt, H. T., and Lubitz, W. (1997) *Biochemistry 36*, 12001−12004.
7. Kamlowski, A., Altenberg-Greulich, B., van der Est, A., Zech, S. G., Bittl, R., Fromme, P., Lubitz, W., and Stehlik, D. (1998) *J. Phys. Chem. B 102*, 8278−8288.
8. Zech, S. G., Hofbauer, W., Kamlowski, A., Fromme, P., Stehlik, D., Lubitz, W., and Bittl, R. (2000) *J. Phys. Chem. B 104*, 9728−9739.
9. Johnson, T. W., Shen, G., Zybailov, B., Kolling, D., Reategui, R., Beauparlant, S., Vassiliev, I. R., Bryant, D. A., Jones, A. D., Golbeck, J. H., and Chitnis, P. R. (2000) *J. Biol. Chem. 275*, 8523−8530.
10. Zybailov, B., van der Est, A., Zech, S. G., Teutloff, C., Johnson, T. W., Shen, G., Bittl, R., Stehlik, D., Chitnis, P. R., and Golbeck, J. H. (2000) *J. Biol. Chem. 275*, 8531−8539.
11. Semenov, A. Y., Vassiliev, I. R., van Der Est, A., Mamedov, M. D., Zybailov, B., Shen, G., Stehlik, D., Diner, B. A., Chitnis, P. R., and Golbeck, J. H. (2000) *J. Biol. Chem. 275*, 23429−22438.
12. Depew, M. C., and Wan, J. K. S. (1988) in *The Chemistry of the Quinonoid Compounds* (Patai, S., and Rappoport, Z., Eds.) pp 963−1018, John Wiley and Sons, New York.
13. Shen, G. Z., Boussiba, S., and Vermaas, W. F. J. (1993) *Plant Cell 5*, 1853−1863.
14. Shen, G. Z., and Bryant, D. A. (1995) *Photosynth. Res. 44*, 41−53.
15. MacKinney, G. (1941) *J. Biol. Chem. 140*, 315−322.
16. Golbeck, J. H. (1995) in *CRC Handbook of Organic Photochemistry and Photobiology* (Song, P. S., and. Horspeels, W., Eds.) pp 1407−1419, CRC Press, Boca Raton, FL.
17. Schagger, H. (1987) *Anal. Biochem. 166*, 368−379.
18. Blum, H., Beier, H., and Gross, H. J. (1987) *Electrophoresis 8*, 93−99.
19. Jung, Y. S., Yu, L., and Golbeck, J. H. (1995) *Photosynth. Res. 46*, 249−255.
20. Zhao, J., Li, R., and Bryant, D. A. (1998) *Anal. Biochem. 264*, 263−270.
21. Fillat, M., Borrias, W., and Weisbeek, P. (1991) *Biochem. J. 280*, 187−191.
22. Yang, F., Shen, G., Schluchter, W. M., Zybailov, B. L., Ganago, A. O., Vassiliev, I. R., Bryant, D. and Golbeck, J. H. (1998) *J. Phys. Chem 102*, 8288−8299.
23. Vassiliev, I. R., Jung, Y. S., Mamedov, M. D., Semenov, A. Y., and Golbeck, J. H. (1997) *Biophys. J. 72*, 301−315.
24. Van der Est, A., Bock, C., Golbeck, J., Brettel, K., Sétif, P., and Stehlik, D. (1994) *Biochemistry 33*, 11789−11797.
25. Rigby, S. E. J., Evans, M. C. W., and Heathcote, P. (1996) *Biochemistry 35*, 6651−6656.
26. Carrington, A., and McLachlan, A. D. (1967) *Introduction to Magnetic Resonance with Applications to Chemistry and Chemical Physics*, Harper and Row, New York.
27. Leibl, W., Toupance, B., and Breton, J. (1995) *Biochemistry 34*, 10237−10244.
28. Kandrashkin, Y., Salikhov, K., van der Est, A., and Stehlik, D. (1998) *Appl. Magn. Res. 15*, 417−447.
29. Kaneko, T., Sato, S., Kotani, H., Tanaka, A., Asamizu, E., Nakamura, Y., Miyajima, N., Hirosawa, M., Sugiura, M., Sasamoto, S., Kimura, T., Hosouchi, T., Matsuno, A., Muraki, A., Nakazaki, N., Naruo, K., Okumura, S., Shimpo, S., Takeuchi, C., Wada, T., Watanabe, A., Yamada, M., Yasuda, M., and Tabata, S. (1996) *DNA Res. 3*, 109−136.
30. Kaneko, T., Sato, S., Kotani, H., Tanaka, A., Asamizu, E., Nakamura, Y., Miyajima, N., Hirosawa, M., Sugiura, M., Sasamoto, S., Kimura, T., Hosouchi, T., Matsuno, A., Muraki, A., Nakazaki, N., Naruo, K., Okumura, S., Shimpo, S., Takeuchi, C., Wada, T., Watanabe, A., Yamada, M., Yasuda, M., and Tabata, S. (1996) *DNA Res. 3*, 185−209.
31. Fujita, Y. (1997) *Photosynth. Res. 53*, 83−93.
32. O'Malley, P. J. (1999) *Biochim. Biophys. Acta 1411*, 101−113.
33. Swallow, A. J. (1982) in *Functions of Quinones in Energy Conserving Systems*, pp 59−72, Academic Press, New York.
34. Iwaki, M., and Itoh, S. (1991) *Biochemistry 30*, 5347−5352.
35. Iwaki, M., and Itoh, S. (1994) *Plant Cell Physiol. 35*, 983−993.
36. Prince, R. C., Dutton, P. L., and Bruce, J. M. (1983) *FEBS Lett. 160*, 273−276.
37. Gutmann. (1976) *Coordination Chem. Rev. 18*, 225−255.
38. Moser, C. C., Keske, J. M., Warncke, K., Farid, R. S., and Dutton, P. L. (1992) *Nature 355*, 796−802.
39. Klukas, O., Schubert, W. D., Jordan, P., Krauss, N., Fromme, P., Witt, H. T., and Saenger, W. (1999) *J. Biol. Chem. 274*, 7361−7367.
40. Vos, M. H., and Van Gorkom, H. J. (1990) *Biophys. J. 58*, 1547−1555.
41. Chamorovskii, S. K., and Cammack, R. (1983) *Biofizika 28*, 549−554.
42. Brettel, K. (1997) *Biochim. Biophys. Acta 1318*, 322−373.
43. Schubert, W. D., Klukas, O., Saenger, W., Witt, H. T., Fromme, P., and Krauss, N. (1998) *J. Mol. Biol. 280*, 297−314.

BI011297W